Carbonation of Hydrous Materials at the Molecular Level: a ToF-SIMS, Raman and DFT study

Giovanni L. Pesce[1,4 i], *Ian W. Fletcher*[2, i1], *James Grant*[3], *Marco Molinari*[3,5], *Stephen C. Parker*[3,*], *Richard J. Ball*[1,*]

[1] University of Bath, Department of Architecture and Civil Engineering, Bath, BA2 7AY, UK

[2] Intertek Wilton Laboratory, The Wilton Centre, Redcar, TS10 4RF, UK

[3] University of Bath, Department of Chemistry, Bath, BA2 7AY, UK

[4]Department of Architecture and Built Environment, Northumbria University, Newcastle upon Tyne, NE1 8ST, UK.

[5]Department of Chemistry, University of Huddersfield, Queensgate, Huddersfield, HD1 3DH, UK

* Corresponding authors: Stephen C. Parker, S.C.Parker@bath.ac.uk, phone: +44 (0)1225 386505; Richard J. Ball, R.J.Ball@bath.ac.uk; phone: +44 (0)1225 309 6944

[1] Currently at Northumbria University, Department of Architecture and Built Environment, Newcastle upon Tyne, NE1 8ST, UK

[ii] Currently at Newcastle University, School of Mechanical and Systems Engineering, Newcastle upon Tyne, NE1 7RU, UK

ToF-SIMS sample preparation

The samples for TOFSIMS were prepared in a glovebox under dry nitrogen (BOC Nitrogen Oxygen Free) and mounted onto the adhesive side of a piece of Sellotape that was attached to a clean stainless steel substrate *ca*. 1cm × 1cm in size by a small piece of double-sided tape (3M 'Scotch Tape' grade 665). A small pile of powder was pressed onto the tape using a clean stainless steel micro spatula. Any excess powder was removed by gentle tapping and blowing using an ambient atmosphere duster. This assembly was subsequently attached to the base plate of a sample holder using a small piece of double-sided tape. The prepared sample was then sealed under nitrogen inside a container and transferred to the TOFSIMS instrument.

ToF-SIMS data analysis

TOFSIMS peaks with a peak area of at least 1000 counts for ionic species with mass up to 117 Dalton were considered in the study. This allowed limiting uncertainty below 3.3% and the number of ionic species to be analysed (a list of species considered in the study is reported in

Table S2 of the SI). The sum of all species with positive polarity used in the analysis accounted for 20.15%-29.23% of the related total counts, whereas the sum of all species with negative polarities accounted for 63.31%-77.55% of the related total counts. The raw data were corrected to take account of any instrumental drifts by dividing the counts of each ionic species by the total counts in the spectrum. To allow easier identification of peaks with highest counts, the data were normalized to the species with the highest count, after the initial correction.

Ionic ratios of similar species containing ^{16}O and ^{18}O were studied using the data normalized to the total counts for both, positive and negative polarity. All ionic species included in the evaluation of the ^{18}O:^{16}O ratio are listed in Table S3. To estimate the total ^{18}O:^{16}O ratio, the

normalized intensity of each specie was multiplied by the number of oxygen isotopes in the specie. Species containing both isotopes were not included in the calculations. The resulting values were summarised to allow calculation of the ^{18}O:^{16}O ratio.

ToF-SIMS results: analysis of the individual ionic species

Figure S1-S3 in the SI show the normalized intensities of ions containing different oxygen isotopes, over the course of the experiment. Data at time 0 refers to the analysis carried out after 3 minutes exposure to atmosphere. Results demonstrate that, within the first 24 hours, the intensity of positive ions containing both, Ca and ^{16}O increases, whereas positive ions containing only ^{16}O and ^{16}OH decrease. At the same time, the intensity of most positive ions containing ^{18}O decreases, with the exception of the $[Ca_2{}^{18}O_2]^+$ which shows a small increase. The intensity of negative species containing ^{16}O increase with the exception of $Ca^{16}OH$, which decreases. Conversely, the intensity of the $[^{18}O]^-$ and $[^{18}OH]^-$ ions decrease.

From day 1 to day 8, the intensity of ions with positive and negative polarity typically showed very little variation. Exceptions are the positive species $[^{18}O]^+$ and $[^{18}OH]^+$, which sharply decrease and increase, respectively. The negative the species $[C^{18}O_3]^-$ and $[HC^{18}O_3]^-$ show a significant increase.

From day 8 to day 137, the most substantial variations are related to ions with positive polarity containing ^{16}O (^{16}O, ^{16}OH, $Ca^{16}OH$, $Ca_2{}^{16}O_2$ and $Ca_2{}^{16}O_2H$), which varied in the range 10^{-2}-10^0, the ions $[^{16}O]^-$ and $[^{16}OH]^-$ with variations within the range 10^{-1}-10^0, and the ions $[^{18}O]^-$ and $[^{18}OH]^-$, which showed variations in the range 10^{-1}-10^{-3}.

Overall, the results show a general reduction in the relative intensities of species containing ^{18}O from time 0 to day 1 and a simultaneous increase of the intensities of species containing ^{16}O. The most relevant variations were related to ions such as $[Ca^{16}OH]^+$, $[Ca_2{}^{16}O_2H]^+$, $[^{16}O]^-$ and $[^{16}OH]^-$. Species containing carbon such as $[HC^{18}O_3]^-$, $[C^{18}O_3]^-$ and $[HC^{16}O_2]^+$ show an increase from day 1 to day 137.

TOFSIMS: analysis of the ^{18}O:^{16}O ratio

Figure S4 shows the ratio of the different isotope species containing ^{18}O and ^{16}O considered in this work. Species with positive polarity showed a general reduction from day 0 to day 1, whereas from day 1 to day 8 and from day 8 to day 137 the ratio remained almost unchanged. Unlike other results, $[^{18}OH:^{16}OH]^+$ ratio of the carbonated $Ca(^{18}OH)_2$ shows an increase from day 1 to day 137, due to an increase in the intensity of the 18OH ion and a simultaneous reduction of the ^{16}OH ions. From day 8 to day 137, the isotopic ratio $[^{18}O:^{16}O]^+$ approaches the values of natural samples.

PHREEQC calculations

Script S1 represent the model is used to calculate OH^- concentration of a solution of pure water in equilibrium with air at 23°C, and of a saturated aqueous solution of $CaOH)_2$ in equilibrium with air. Lines 1-10 are specially designed to not allow the N_2 gas contained in the air to react with O and form NO_3, according to a model suggested by David Parkhurst[12]. Absence of these lines would make the N_2 and O_2 in the air react to form NO_3 since, having a fixed partial pressures of N_2 and O_2 would generates huge amounts of NO_3, and the program would fail to converge. Lines 12 to19 are used to model a solution made of pure water at 23°C. Initial pH 7 is adjusted during calculations to achieve charge balance. Lines 21 to 25 are used to model an equilibrium phase simulating air that is made to reacted with the water solution. Lines 28 to 21 are used to model an infinite reservoir of $Ca(OH)_2$ to be reacted with the water in equilibrium with air. The $Ca(OH)_2$ is forced to be in equilibrium with the solution. Values of the OH^- concentration can be read at the end of each batch-reaction calculation. Values are reported in Table S5 of these SI, together with the related pH. Databases used for these calculations are the wateq4f.dat (a database suited for processing

large numbers of water analyses) and the llnl.dat (a database that uses thermodynamic data compiled by the Lawrence Livermore National Laboratory). Results obtained with the llnl.dat database are in very good agreement with the experimentally verified previous calculations made with a different model and the same llnl.dat database.[13]

Script S1 - PHREEQC model used to calculate OH^- concentration in different aqueous solutions

```
SOLUTION_MASTER_SPECIES
   Ngas    Ngas2    0    Ngas2    14
SOLUTION_SPECIES
   Ngas2 = Ngas2
   LogK  0.0
PHASES
   Ngas
       Ngas2 = Ngas2
       log_k           -3.260
       delta_h -1.358  kcal

SOLUTION 1 Pure water
 temp 23
 pH 7    charge
 pe 4
 redox pe
 units mol/kgw
 density 1
 -water 1 # kg

EQUILIBRIUM_PHASES 1 # Air to be in equilibrium with water
 Ngas   -0.1079
 O2(g)  -0.6990
 CO2(g) -3.3979 # 400ppm
SAVE solution 1
END

EQUILIBRIUM_PHASE 2 # Portlandite to be in equilibrium with solution 1
  Portlandite 0 1000 # Infinite reservoir in equilibrium with solution
USE solution 1
END
```

Figures

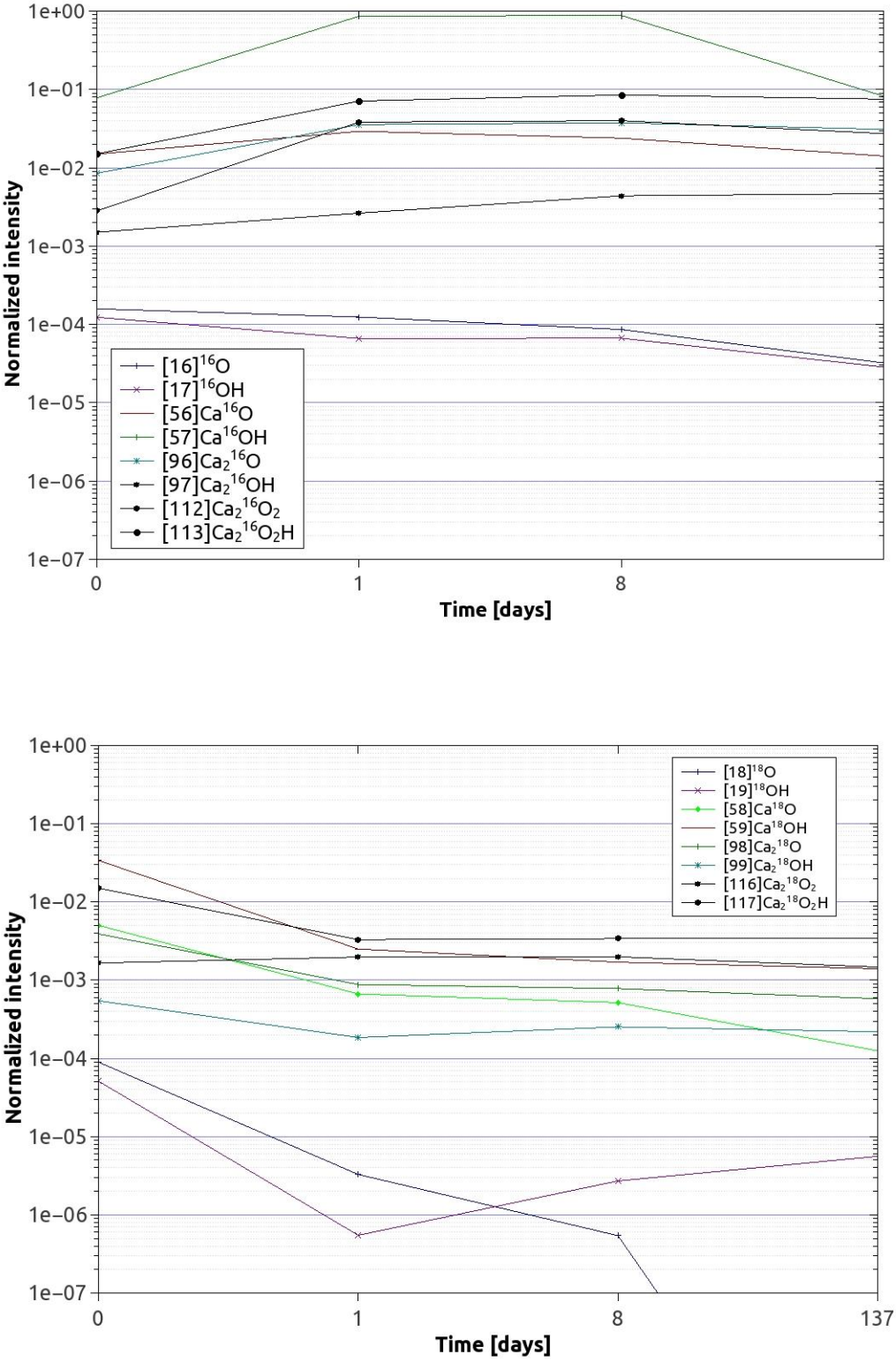

Figure S1 - Positive ions containing ^{16}O (above) and ^{18}O (below). Numbers next to the chemical formula in the key represent the ionic mass in Dalton. Time 0 refers to the analysis after 3'

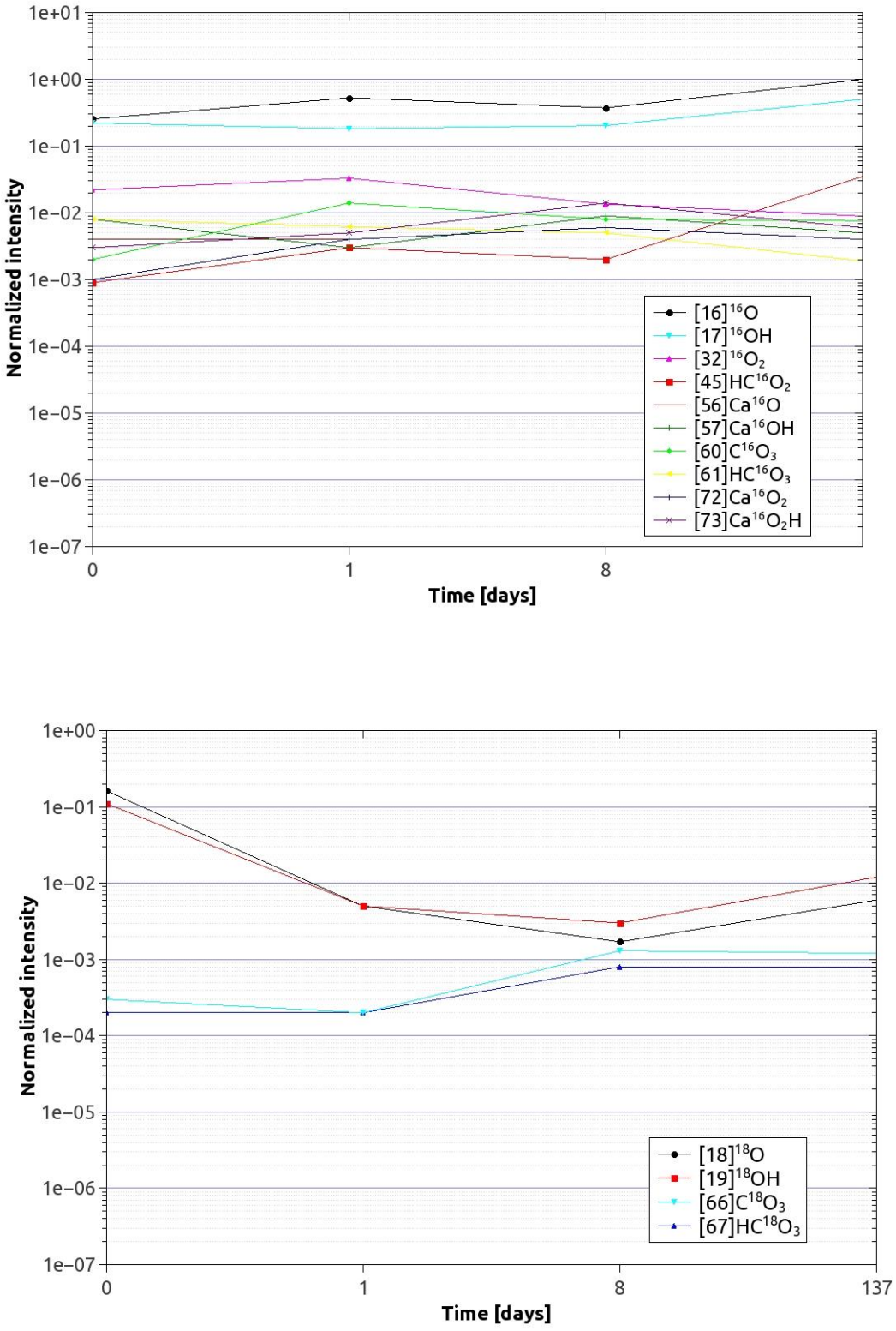

Figure S2 - Negative ions containing ^{16}O (above) and ^{18}O (below). Numbers next to the chemical formula in the key represent the ionic mass in Dalton. Time 0 refers to the analysis after 3'

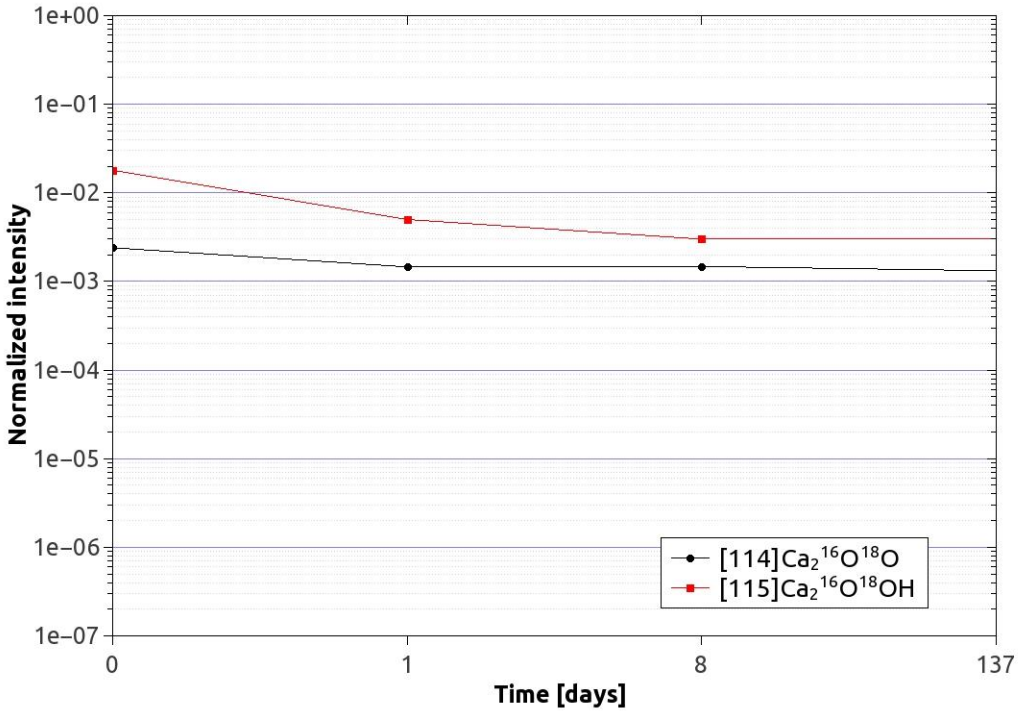

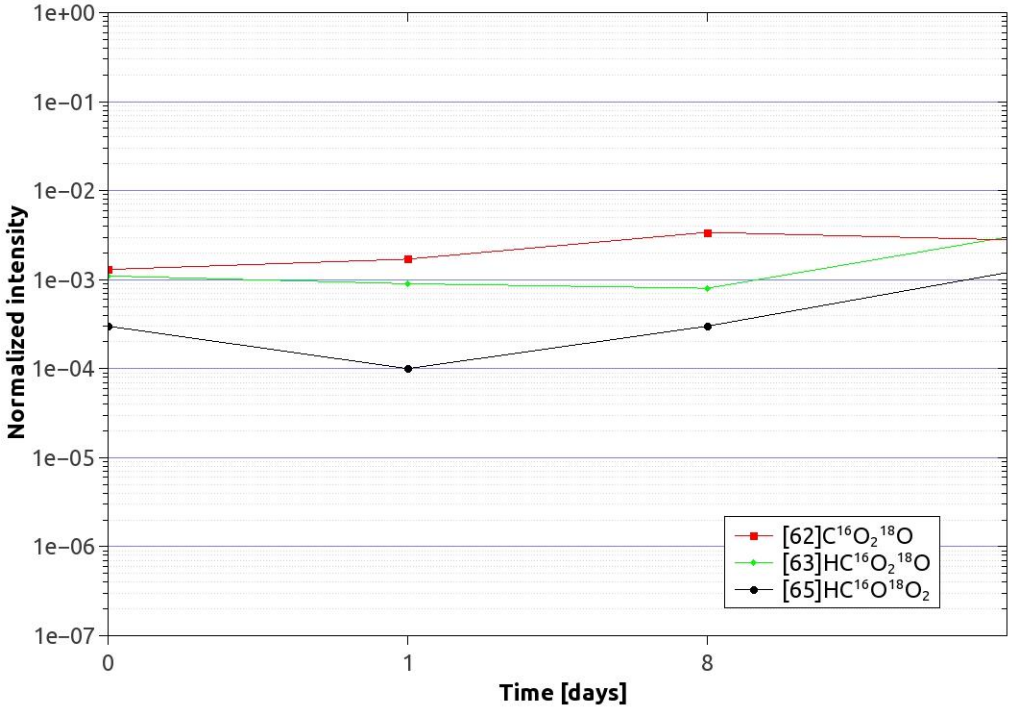

Figure S3 - Positive (above) and negative (below) ions containing both, ^{16}O and ^{18}O. Numbers next to the chemical formula in the key represent the ionic mass in Dalton. Time 0 refers to the analysis after 3'

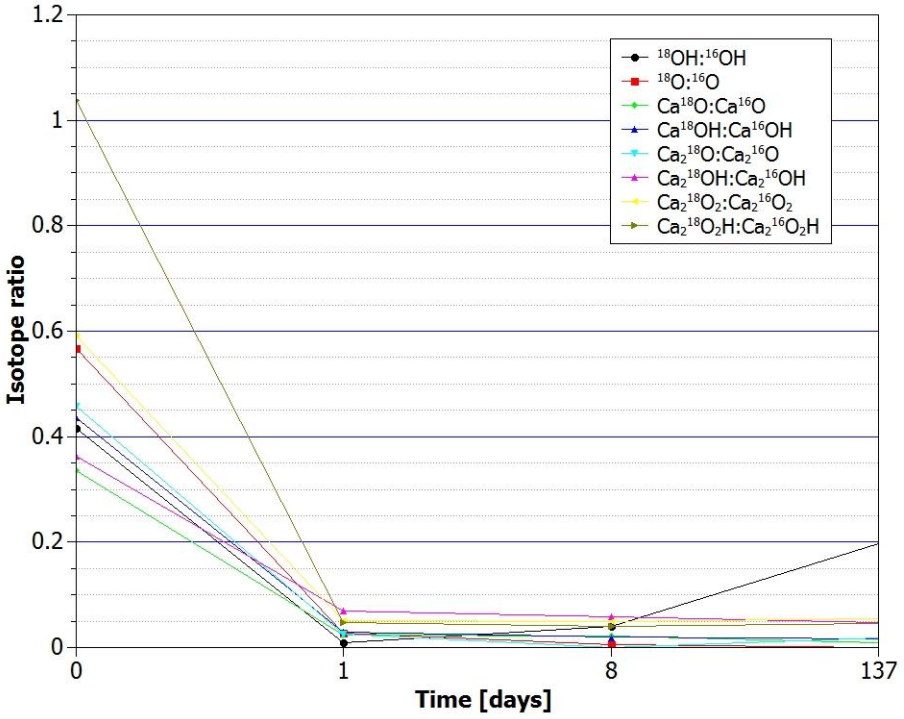

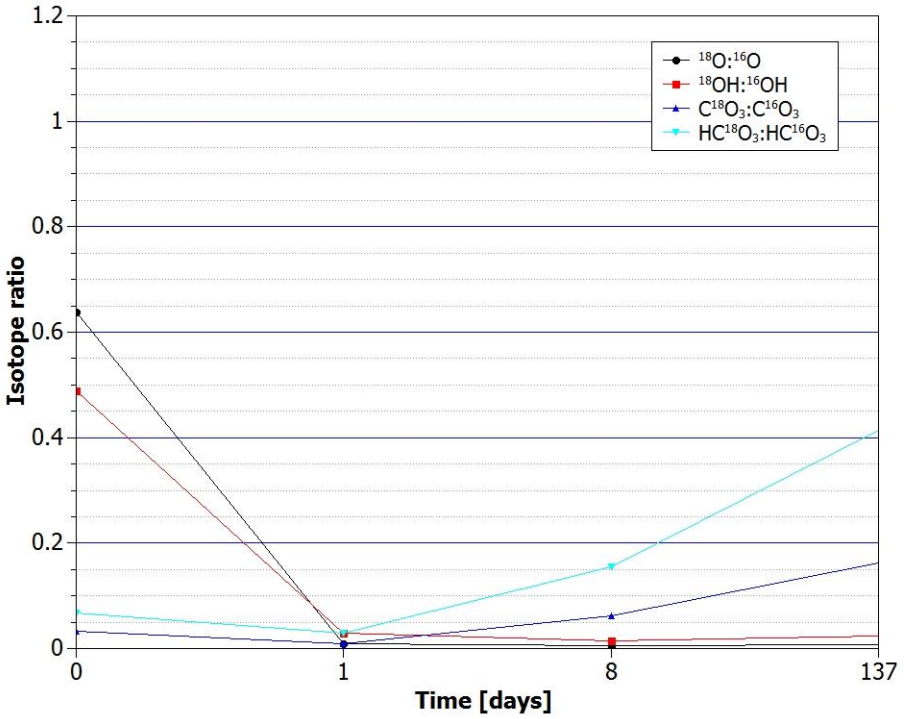

Figure S4 - Change over time of the isotope ratio between similar ions containing ^{18}O and ^{16}O. Positive ions on the top, negative ions at the bottom. Time 0 refers to the analysis after 3'

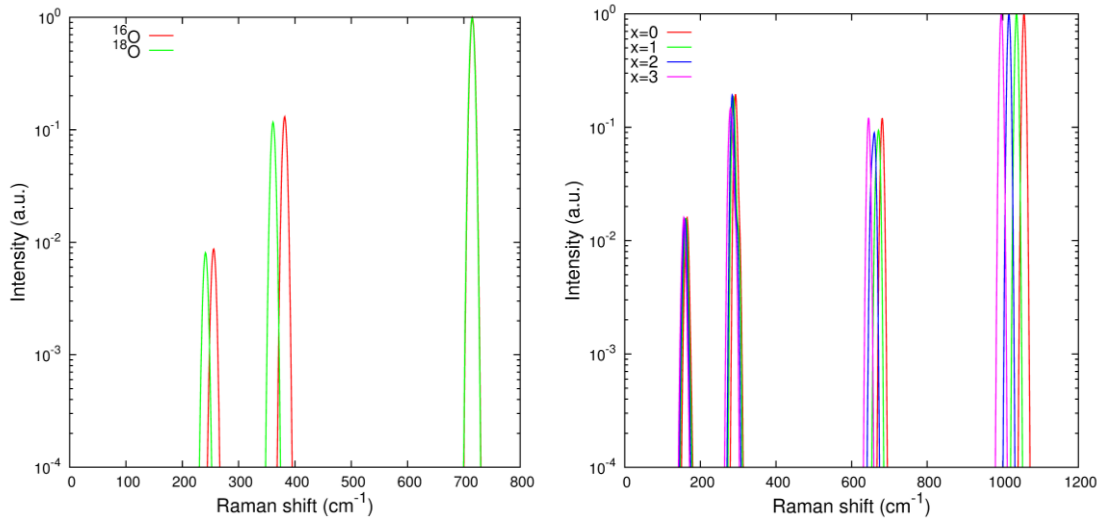

Figure S5 - Predicted isotopic dependence of Raman shift in portlandite (left) and calcite (right). The predicted shifts in peaks are shown for 100% substitution of 18O in portlandite while for calcite spectra are with all carbonates ions containing 0, 1, 2, and 3 18O isotopes.

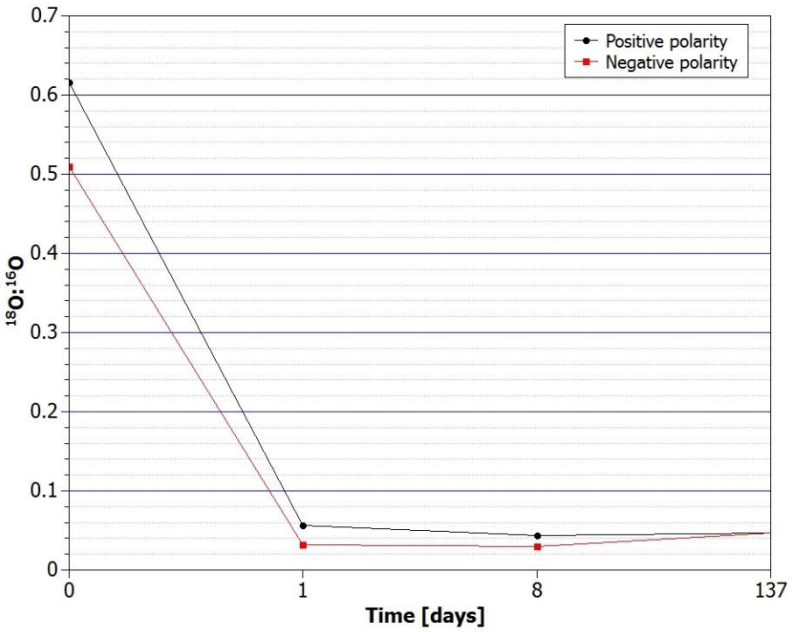

Figure S6 – Variation of the total 18O:16O ratio over the time of the test

Tables

Table S1 - Table of experimental and simulated lattice parameters for portlandite. Experimental data from: Desgranges, L., Grebille, D., Calvarin, G., Chevrier, G., Floquet, N., Niepce, J.C., Acta Crystallographica, Section B: Structural Science (1993) 49, p812-p817

Vector	Experiment (Å)	Simulation (Å)	Error
a,b	3.589	3.573	0.4%
c	4.911	4.794	2.4%

Table S2 – List of ions analysed in this study. Table is ordered by ionic mass and is divided into ions with positive and negative polarity. Only the oxygen isotopes are highlighted. ToFSIMS signal of the species listed in this table had at least 1000 counts

Mass [Da]	Positive polarity	Negative polarity
16	^{16}O	^{16}O
17	^{16}OH	^{16}OH
18	^{18}O	^{18}O
19	^{18}OH	^{18}OH
32	-	$^{16}O_2$
45	-	$HC^{16}O_2$
56	$Ca^{16}O$	$Ca^{16}O$
57	$Ca^{16}OH$	$Ca^{16}OH$
58	$Ca^{18}O$	-
59	$Ca^{18}OH$	-
60	-	$C^{16}O_3$
61	-	$HC^{16}O_3$
62	-	$C^{16}O_2{}^{18}O$
63	-	$HC^{16}O_2{}^{18}O$
65	-	$HC^{16}O^{18}O_2$
66	-	$C^{18}O_3$
67	-	$HC^{18}O_3$
72	-	$Ca^{16}O_2$
73	-	$Ca^{16}O_2H$
96	$Ca_2{}^{16}O$	-
97	$Ca_2{}^{16}OH$	-
98	$Ca_2{}^{18}O$	-
99	$Ca_2{}^{18}OH$	-
112	$Ca_2{}^{16}O_2$	-
113	$Ca_2{}^{16}O_2H$	-
114	$Ca_2{}^{16}O^{18}O$	-
115	$Ca_2{}^{16}O^{18}OH$	-
116	$Ca_2{}^{18}O_2$	-
117	$Ca_2{}^{18}O_2H$	-

Table S3 - Ionic species for which the isotope ratio $^{18}O/^{16}O$ was calculated

Polarity	Ionic ratio
Positive	O
	OH
	CaO
	CaOH
	Ca_2O
	Ca_2OH
	Ca_2O_2
	Ca_2O_2H
Negative	O
	OH
	CO_3
	HCO_3

Table S4 - Peak positions in the Raman spectra for different phases of calcium carbonate reported in the scientific literature

CALCITE							
Reference	v_1		v_4		-	-	-	-
Kim et a;. (1)	1088		713		281			
Weiner et al. (2)	1086		712		282	156		
Noel et al. (3)	1085		711		282	154		
Kontoyannis et al. (4)	1085		711		280	154		
Nehrke et al. (5)	1085		711		282	155		
ARAGONITE								
Reference	v_1		v_4		-	-	-	-
Weiner et al. (2)	1085		703		206	155		
Gauldie et al. (6)	1084		701-705		205	152		
	1085		701-705					
Kontoyannis et al. (4)	1084		700-705		205	152		
Tomas et al. (7)					204	152		
Nehrke et al. (5)	1085		705		206	155		
VATERITE								
Reference	v_1		v_4		-	-	-	-
Kim et al. (1)	1095	1064						
Noel et al. (3)	1095	1064	754	713				
Gauldie et al. (6)	1090	1075	751	740	301	266	207	106-115
	1084	1066	752	713				
Kontovannis et al. (4)	1089	1074	750	738	301	268		118
Tomas et al. (7)					301	266		106
Nehrke et al. (5)	1090	1075	750	740	300	267	114	105
Hu et al. (8)	1090	1075	752	742				
IKAITE								
Reference	v_3		v_1		v_4	-	-	-
Hu et al. (8)			1071		718			
Tlili et al. (9)			1073		722			
	1410		1070		718	534	507	
MONO-HYDRO CALCITE								
Reference	v_3		v_1		v_2	v_4	-	-
Tlili et al. (9)	1403, 1480		1066		873	694, 719	590, 780	
			1069		725			
	107, 1486		1063		872	700, 726	590, 674, 765	
AMORPHOUS CALCIUM CARBONATE								
Reference	v_3		v_1		v_2	v_4	-	-
Ihli et al. (1)0			1088					
Kim et al. (1)			1084					
Lee et al. (11)			1080					
Weiner et al (2)			1085					
Noel et al. (3)			1085					
Tlili et al. (9)	1390-1460		1077		868	968, 723	932, 846, 638, 583	
			1083					

Table S5 – pH and OH- concentration in different aqueous solutions, calculated using PHREEQC

Solution	Database wateq4f.dat		
	pH	OH^- Molality	OH^- Activity
Pure H_2O in equilibrium with air	5.6	3.444E-09	3.438E-09
$Ca(OH)_2$ saturated aqueous solution	12.54	3.697E-02	2.988E-02

	Database llnl.dat		
	pH	OH^- Molality	OH^- Activity
Pure H_2O in equilibrium with air	5.6	3.353E-09	3.347E-09
$Ca(OH)_2$ saturated aqueous solution	12.45	2.801E-02	2.321E-02

References

1) Kim, Y.-Y.; Kulak, A. N.; Li, Y.; Batten, T.; Kuball, M.; Armes, S. P. & Meldrum, F. C. Substrate-directed formation of calcium carbonate fibres *J. Mater. Chem., The Royal Society of Chemistry,* **2009***, 19*, 387-398

2) Weiner, S.; Levi-Kalisman, Y.; Raz, S. & Addadi, L. Biologically Formed Amorphous Calcium Carbonate, *Connective Tissue Research*, **2003**, 44:1, 214-218

3) Noel, E. H.; Kim, Y.-Y.; Charnock, J. M. & Meldrum, F. C. Solid state crystallization of amorphous calcium carbonate nanoparticles leads to polymorph selectivity. *CrystEngComm,* **2013***, 15*, 697-705

4) Kontoyannis, C. G. & Vagenas, N. V. Calcium carbonate phase analysis using XRD and FT-Raman spectroscopy. *Analyst,* **2000***, 125*, 251-255

5) Nehrke, G.; Poigner, H.; Wilhelms-Dick, D.; Brey, T. & Abele, D. Coexistence of three calcium carbonate polymorphs in the shell of the Antarctic clam Laternula elliptica. *G3*, **2012**, 13, 5, 1-8

6) Gauldie, R. W.; Sharma, S. K. & Volk, E. Micro-Raman Spectral Study of Vaterite and Aragonite Otoliths of the Coho Salmon, Oncorhynchus kisutch *Comparative Biochemistry and Physiology -- Part A: Physiology,* **1997***, 118*, 753-757

7) Tomás, J. & Geffen, A. J. Morphometry and composition of aragonite and vaterite otoliths of deformed laboratory reared juvenile herring from two populations. *Journal of Fish Biology, Blackwell Science Ltd,* **2003***, 63*, 1383-1401

8) Hu, Y. B.; Wolf-Gladrow, D. A.; Dieckmann, G. S.; Völker, C. & Nehrke, G. A laboratory study of ikaite ($CaCO_3 \cdot 6H_2O$) precipitation as a function of pH, salinity, temperature and phosphate concentration. *Marine Chemistry*, **2014**, 162, 10-18

9) Tlili, M. M.; Ben Amor, M.; Gabrielli, C.; Joiret, S.; Maurin, G.; & Rousseau, P. Characterization of $CaCO_3$ hydrates by micro-Raman spectroscopy. *J. Raman Spectrosc*. **2001,** 33, 10–16

10) Ihli, J.; Kulak, A. N. & Meldrum, F. C. Freeze-drying yields stable and pure amorphous calcium carbonate (ACC) *Chem. Commun.,* **2013***, 49*, 3134-3136

11) Lee, K.; Wagermaier, W.; Masic, A.; Kommareddy, K. P.; Bennet, M.; Manjubala, I.; Lee, S.-W.; Park, S. B.; Cölfen, H. & Fratzl, P. Self-assembly of amorphous calcium carbonate microlens arrays. *Nat Commun,* **2012***, 3*, 725

12) http://phreeqcusers.org/index.php?topic=67.0

13) Serrapede, M.; Pesce, G.L.; Ball, R.J.; Denuault, G. Nanostructured Pd hydride microelectrodes: In situ monitoring of pH variations in a porous medium. *Analytical Chemistry*. **2014**, 86 (12), 5758-5765